Supplementary Material for "Polar flocks with discretized directions: the active clock model approaching the Vicsek model"

Swarnajit Chatterjee,[1,*] Matthieu Mangeat,[1,†] and Heiko Rieger[1,2,‡]

[1] *Center for Biophysics & Department of Theoretical Physics, Saarland University, 66123 Saarbrücken, Germany.*

[2] *INM – Leibniz Institute for New Materials, Campus D2 2, 66123 Saarbrücken, Germany.*

I. q-STATE ACM ON DISCRETE LATTICES

A. The Model

We consider an ensemble of N particles defined on periodic 2d lattices with $L_x \times L_y$ sites. The average particle density in the system is $\rho_0 = N/(L_x L_y)$. Each particle endowed with a spin state (or clock angle) $\theta \in \{0, 2\pi/q, 4\pi/q, \cdots, 2(q-1)\pi/q\}$ can either flip to a different spin-state θ' or jump to a nearest neighbour lattice site probabilistically. The spin-state of the k-th particle on site i is denoted θ_i^k. The number of particles on site i is denoted by ρ_i with no restriction on its value, and the magnetization on site i reads

$$\mathbf{m}_i = \sum_{k=1}^{\rho_i} \cos\theta_i^k \ \mathbf{e_x} + \sum_{k=1}^{\rho_i} \sin\theta_i^k \ \mathbf{e_y}. \tag{S1}$$

The flip probabilities of the ACM are derived from a ferromagnetic Hamiltonian $H_{\mathrm{ACM}} = \sum_i H_i$ decomposed as the sum of local Hamiltonian H_i, taken from the standard clock model:

$$H_i = -\frac{J}{2\rho_i} \sum_{k=1}^{\rho_i} \sum_{l \neq k} \cos(\theta_i^k - \theta_i^l) \tag{S2}$$

where the prefactor $1/2\rho_i$ makes the Hamiltonian intensive and avoids the double counting of interactions and J is the coupling constant between particles. When $q = 2$, we recover the Hamiltonian defined for the AIM. Consider now a spin flip of a single particle on site i from state θ to state θ'. Without any loss of generality we can suppose that the l^{th} particle flips. Only the on-site energy is changed, leading to an energy difference between the new and the old state:

$$\Delta H = -\frac{J}{\rho_i} \sum_{k=1, k\neq l}^{\rho_i} \left[\cos(\theta_i^k - \theta') - \cos(\theta_i^k - \theta)\right] \tag{S3}$$

$$= -\frac{J}{\rho_i} \sum_{k=1, k\neq l}^{\rho_i} \left[\cos\theta_i^k(\cos\theta' - \cos\theta) + \sin\theta_i^k(\sin\theta' - \sin\theta)\right]. \tag{S4}$$

Defining the conserved quantity during the flip

$$\boldsymbol{\mu}_i = \sum_{k=1, k\neq l}^{\rho_i} \cos\theta_i^k \ \mathbf{e_x} + \sum_{k=1, k\neq l}^{\rho_i} \sin\theta_i^k \ \mathbf{e_y}, \tag{S5}$$

we get the energy difference:

$$\Delta H = -\frac{J}{\rho_i} \boldsymbol{\mu}_i \cdot (\mathbf{e}_{\theta'} - \mathbf{e}_\theta). \tag{S6}$$

*Electronic address: swarnajit.chatterjee@uni-saarland.de

†Electronic address: mangeat@lusi.uni-sb.de

‡Electronic address: heiko.rieger@muni-saarland.de

From the Eq. (S1), $\boldsymbol{\mu}_i$ is linked to the magnetization on the site i before the flip $\mathbf{m}_i$ and after the flip $\mathbf{m}'_i$ with the relations $\boldsymbol{\mu}_i = \mathbf{m}_i - \mathbf{e}_\theta = \mathbf{m}'_i - \mathbf{e}_{\theta'}$, which lead to the energy difference:

$$\Delta H = -\frac{J}{\rho_i}\left[\mathbf{m}_i \cdot (\mathbf{e}_{\theta'} - \mathbf{e}_\theta) + 1 - \cos(\theta' - \theta)\right], \tag{S7}$$

used in the main text. The energy difference can also be written as

$$\Delta H = -\frac{J}{2\rho_i}(\mathbf{m}_i + \mathbf{m}'_i) \cdot (\mathbf{e}_{\theta'} - \mathbf{e}_\theta), \tag{S8}$$

with both the magnetizations before and after the flip.

In analogy to the AIM and the APM, the transition rate is chosen to verify the detailed balance:

$$W_{\text{flip}}(\theta, \theta') = \gamma \exp(-\beta \Delta H) = \gamma \exp\left\{\frac{\beta J}{\rho_i}\left[\mathbf{m}_i \cdot (\mathbf{e}_{\theta'} - \mathbf{e}_\theta) + 1 - \cos(\theta' - \theta)\right]\right\}. \tag{S9}$$

Moreover, each particle performs a biased diffusion on the lattice depending on the particle state θ: the hopping rate is $W_{\text{hop}} = D(1 + \varepsilon)$ in the direction θ and $W_{\text{hop}} = D[1 - \varepsilon/(q-1)]$, otherwise.

We perform the numerical simulations with a Monte Carlo algorithm similar to the one used to analyze the active Potts model (APM) [1] using the flip rate derived in Eq. (S9). Here we study the $q = 4$-state ACM and the $q = 6$-state ACM on a 2d square lattice and 2d triangular lattice, respectively. The time is discretized in small time units $\Delta t = [qD + \exp(2\beta J)]^{-1}$ where the time increment is defined as $\Delta t/N$, N being the total number of particles. At each $\Delta t/N$, a randomly chosen particle either flips its state from θ to θ' with probability $W_{\text{flip}}(\theta, \theta')\Delta t$ or hops to a nearest neighbor with probability $W_{\text{hop}}\Delta t$.

B. Numerical Results

Now, we will present numerical results from our simulations of the 4-state ACM. Simulations are performed on a 100×100 square lattice using three control parameters: the temperature $T = \beta^{-1}$, the average particle density ρ_0, and the bias ε.

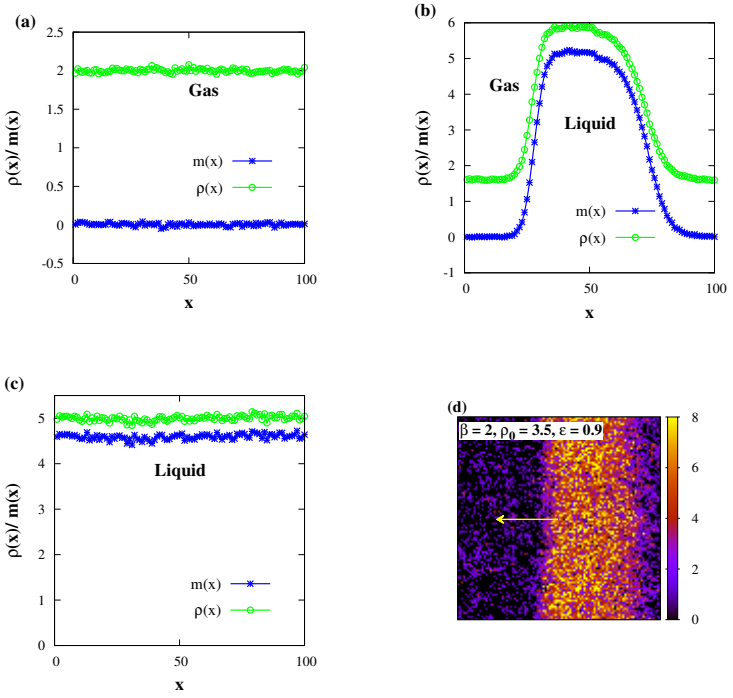

FIG. S1: (color online) Three phases of the 4-state ACM for $\varepsilon = 0.9$, (a) disordered gas for $\beta = 1.2$, $\rho_0 = 2$, (b) liquid-gas co-existence for $\beta = 2$, $\rho_0 = 3.5$, and (c) polar liquid for $\beta = 2.3$, $\rho_0 = 5$. (d) Density field snapshot corresponding to (b).

The three typical phases of the ACM are shown in Fig. S1 for $\varepsilon = 0.9$. A disordered gaseous phase at high temperature and low density ($\beta = 1.2$, $\rho_0 = 2$) in Fig. S1(a) are followed by a liquid-gas co-existence phase in Fig. S1(b) for intermediate temperature and density ($\beta = 2$, $\rho_0 = 3.5$) and a polar liquid phase in Fig. S1(c) at low temperature and high density ($\beta = 2.3$, $\rho_0 = 5$). In Fig. S1(d), we represent the corresponding snapshot of Fig. S1(b) where a fully phase-separated polar liquid band is shown traveling transversely on a gaseous background. All the profiles presented in Fig. S1(a–c) are averaged over space and time and the two homogeneous phases, gas and liquid, are defined respectively by the average magnetization where for a gas phase $\langle m \rangle \approx 0$ and for the liquid phase, $\langle m \rangle \approx m_0 \neq 0$.

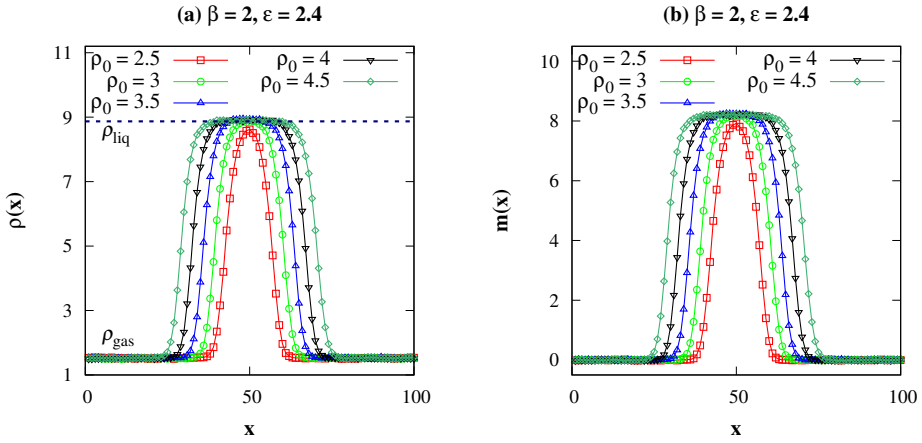

FIG. S2: (color online) Segregated (a) density and (b) magnetization profiles with increasing initial ρ_0 are shown for $\beta = 2$ and $\varepsilon = 2.4$.

Phase-separated density and magnetization profiles (averaged along the y-axis and over time) of the liquid-gas coexistence phase are shown in Fig. S2(a) and Fig. S2(b) respectively, for $\beta = 2, \varepsilon = 2.4$ and several ρ_0. The width of the polar liquid band increases with the average density ρ_0 without affecting the densities of the liquid $\rho_{\rm liq}(T, \varepsilon)$ and the gaseous $\rho_{\rm gas}(T, \varepsilon)$ phases. A single internal state ($\theta = \pi/2$) dominates each of the band, then all these bands are longitudinal in nature.

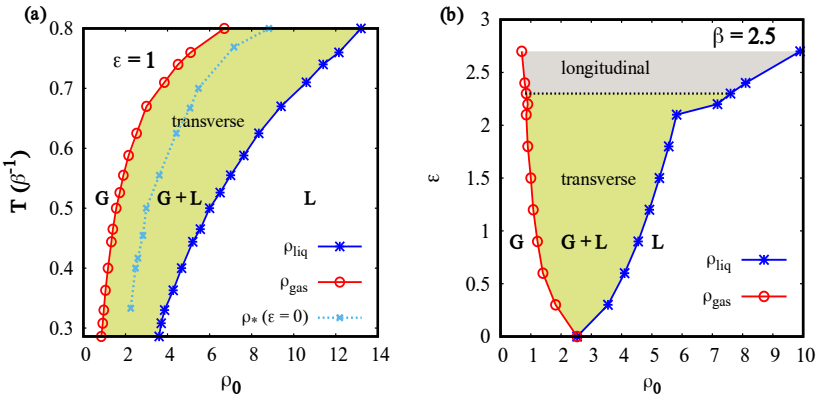

FIG. S3: (color online) Phase diagrams of the 4-state ACM. (a) Temperature-density (T-ρ_0) phase diagram for $\varepsilon = 1$. The dotted line indicates the transition density ρ^* for $\varepsilon = 0$. (b) Velocity-density (ε-ρ_0) diagram for $\beta = 2.5$ where the black dotted line indicates the reorientation transition line from transverse to longitudinal particle motion.

In Fig. S3(a) we show the phase diagram of the 4-state ACM in the (T, ρ_0) plane for $\varepsilon = 1$. The binodals $\rho_{\rm gas}$ and $\rho_{\rm liq}$, which are are computed from the time averaged phase separated density profiles shown in Fig. S2, segregate the gaseous (G), gas-liquid co-existence ($G + L$), and liquid (L) phases. The dashed line inside the co-existence region represents the critical densities $\rho_*(\beta)$ where the liquid-gas transition occurs at $\varepsilon = 0$ (see Fig. S4). The (ε,ρ_0) phase diagram for a fixed temperature $\beta = 2.5$ is shown in Fig. S3(b). $\rho_{\rm gas}$ and $\rho_{\rm liq}$ merges at $\rho_*(\beta = 2.5, \varepsilon = 0) \simeq 2.5$ for $\varepsilon = 0$, which is the critical point. We have already demonstrated in Fig. S1 and Fig. S2 that the 4-state ACM

exhibits the reorientation transition of the co-existence phase and it is depicted in Fig. S3(b) through two different color shades. In the (T, ρ_0) phase diagram we do not observe the longitudinal phase as the diagram is obtained for small particle velocity, $\varepsilon = 1$ for which the system manifests only transverse band motion. In the (ε,ρ_0) phase diagram the transition approximately happens at $\varepsilon \simeq 2.3$ (represented by black dotted line).

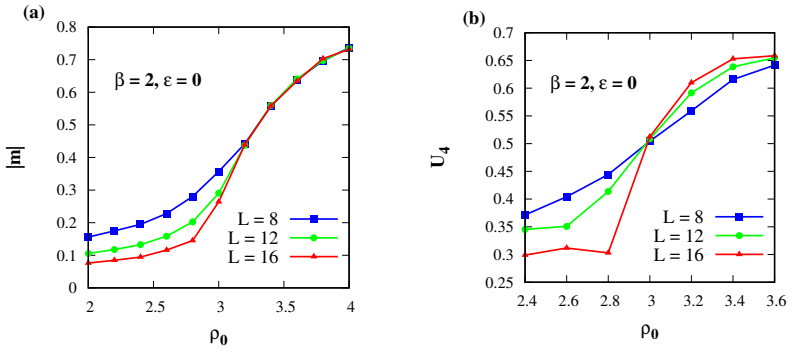

FIG. S4: (color online) Liquid-gas phase transition in 4-state ACM for $\beta = 2$ and $\varepsilon = 0$. (a) Magnetization $|\mathbf{m}|$ versus ρ_0 for different lattice sizes $L = 8$, $L = 12$, and $L = 16$. (b) Binder cumulant U_4 versus ρ_0 for different lattice sizes L. The critical density $\rho_*(\beta = 2) = 2.99 \pm 0.01$ is extracted from the intersection of these curves.

The $\varepsilon = 0$ limit of the ACM is the purely diffusive version of the model where a continuous phase transition is observed from a low-density homogeneous phase to a high-density ordered phase without the gas-liquid coexistence phase as presented in Fig. S4 for $\beta = 2$. Such second order transition was also observed in the AIM [2] but in the APM [1], the transition reported was first order in nature. In Fig. S4(a), the magnetization is plotted against ρ_0 and we observe a smooth, continuous transition from a high magnetized liquid state at larger ρ_0 to a gaseous state at smaller ρ_0. The critical density of this transition, ρ^* is calculated from the Binder cumulant $U_4 = 1 - \langle|\mathbf{m}|^4\rangle/3\langle|\mathbf{m}|^2\rangle^2$ versus ρ_0 shown in Fig. S4(b) and from the intersection of the U_4 curves for different L, we quantified the critical density $\rho_*(\beta = 2) = 2.99 \pm 0.01$.

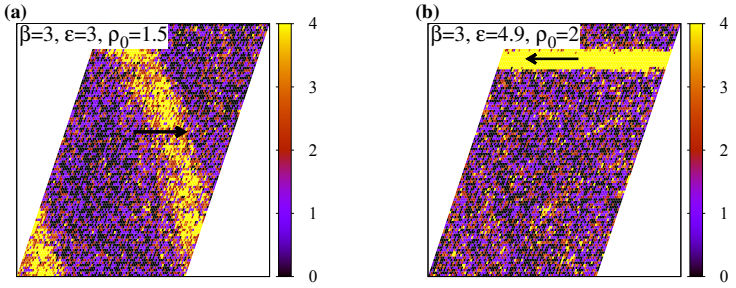

FIG. S5: (color online) Steady-state density snapshots of the 6-state ACM on a triangular lattice of dimension 100×100 showing (a) transverse band motion for $\varepsilon = 3$, $\rho_0 = 1.5$ and (b) longitudinal band motion for $\varepsilon = 4.9$, $\rho_0 = 2$. $\beta = 3$. Colorbar represents site occupation.

Additionally, we present two snapshots of the 6-state ACM on a triangular lattice in Fig. S5(a–b) as a function of ε confirming the band to lane reorientation transition also for $q = 6$. In Fig. S5(a) we show the transverse motion of the polar liquid band for $\varepsilon = 3$, which is constituted by particles having internal state $\theta = 0$ whereas longitudinal lane formation along the predominant direction of the particles with $\theta = \pi$ is observed for $\varepsilon = 4.9$. It was shown in the context of APM [1] that this reorientation transition which was not present in other known flocking models, is not an artefact of any algorithmic implementation and our investigation of the q-state ACM on discrete lattices has validated that argument further.

II. HYDRODYNAMIC DESCRIPTION

Now, we will present the derivation of the hydrodynamic equations (3)-(5) presented in the main text. We define $n(\mathbf{x},\theta;t)$ as the probability density for a particle to be at the position $\mathbf{x}$ and in the spin-state θ at the time t. The particle density reads

$$\rho(\mathbf{x},t)=\int_0^{2\pi}d\theta n(\mathbf{x},\theta;t)=\Delta\theta\sum_\theta n(\mathbf{x},\theta;t) \tag{S10}$$

for the AXYM and the q-state ACM with $\Delta\theta=2\pi/q$, respectively. Similarly, the magnetization is defined by

$$\mathbf{m}(\mathbf{x},t)=\int_0^{2\pi}d\theta\mathbf{e}_\theta n(\mathbf{x},\theta;t)=\Delta\theta\sum_\theta \mathbf{e}_\theta n(\mathbf{x},\theta;t), \tag{S11}$$

with $\mathbf{e}_\theta=(\cos\theta,\sin\theta)$. Note that $\rho(\mathbf{x}_i,t)\equiv\rho_i(t)$ and $\mathbf{m}(\mathbf{x}_i,t)\equiv\mathbf{m}_i(t)$ represents the particle number and the magnetization in the neighborhood $\mathcal{N}_i$, respectively. Finally, we also define the nematic tensor as

$$Q(\mathbf{x},t)=\int_0^{2\pi}d\theta\begin{pmatrix}\cos 2\theta & \sin 2\theta\\ \sin 2\theta & -\cos 2\theta\end{pmatrix}n(\mathbf{x},\theta;t)=\Delta\theta\sum_\theta\begin{pmatrix}\cos 2\theta & \sin 2\theta\\ \sin 2\theta & -\cos 2\theta\end{pmatrix}n(\mathbf{x},\theta;t)\equiv\begin{pmatrix}Q_1(\mathbf{x},t) & Q_2(\mathbf{x},t)\\ Q_2(\mathbf{x},t) & -Q_1(\mathbf{x},t)\end{pmatrix}, \tag{S12}$$

and we suppose that higher harmonic terms are zero.

We derive the master equation corresponding to the microscopic process with hopping rates $W_{\rm hop}(\theta,\phi)$ and flipping rates $W_{\rm flip}(\theta,\theta')$, where θ, ϕ and θ' are the state angle of the particle, the hopping angle and the angle after the flip, respectively. It writes then as

$$\begin{aligned}n(\mathbf{x},\theta;t+dt)=n(\mathbf{x},\theta;t)\left[1-dt\sum_\phi W_{\rm hop}(\theta,\phi)-dt\sum_{\theta'\neq\theta}\frac{W_{\rm flip}(\theta,\theta')}{q-1}\right]\\ +\left[\sum_\phi n(\mathbf{x}-\mathbf{e}_\phi,\theta;t)W_{\rm hop}(\theta,\phi)+\sum_{\theta'\neq\theta}n(\mathbf{x},\theta';t)\frac{W_{\rm flip}(\theta',\theta)}{q-1}\right]dt.\end{aligned} \tag{S13}$$

Taking the limit $dt\to 0$, we get

$$\frac{\partial n}{\partial t}(\mathbf{x})=\sum_\phi\left[n(\mathbf{x}-\mathbf{e}_\phi,\theta)-n(\mathbf{x},\theta)\right]W_{\rm hop}(\theta,\phi)+\frac{1}{q-1}\sum_{\theta'\neq\theta}\left[n(\mathbf{x},\theta')W_{\rm flip}(\theta',\theta)-n(\mathbf{x},\theta)W_{\rm flip}(\theta,\theta')\right]\equiv I_{\rm hop}+I_{\rm flip}. \tag{S14}$$

We can obviously add the term $\theta=\theta'$ in $I_{\rm flip}$. First, we calculate the expression of $I_{\rm hop}$. Using the definition of $W_{\rm flip}$, we obtain

$$I_{\rm hop}=\frac{\overline{D}(1-\overline{\varepsilon})}{q}\sum_\phi\left[n(\mathbf{x}-\mathbf{e}_\phi,\theta)-n(\mathbf{x},\theta)\right]+\overline{D}\overline{\varepsilon}\left[n(\mathbf{x}-\mathbf{e}_\theta,\theta)-n(\mathbf{x},\theta)\right]. \tag{S15}$$

In the hydrodynamic limit, we show that

$$n(\mathbf{x}-\mathbf{e}_\phi,\theta)-n(\mathbf{x},\theta)=-\mathbf{e}_\phi\cdot\nabla n(\mathbf{x},\theta)+\frac{1}{2}\left(\mathbf{e}_\phi\cdot\nabla\right)^2 n(\mathbf{x},\theta)+\cdots, \tag{S16}$$

and we deduce then

$$\sum_\phi\left[n(\mathbf{x}-\mathbf{e}_\phi,\theta)-n(\mathbf{x},\theta)\right]=\frac{q}{4}\nabla^2 n(\mathbf{x},\theta). \tag{S17}$$

The hopping term becomes

$$I_{\rm hop}=\frac{\overline{D}(1-\overline{\varepsilon})}{4}\nabla^2 n(\mathbf{x},\theta)+\frac{\overline{D}\overline{\varepsilon}}{2}\left(\mathbf{e}_\theta\cdot\nabla\right)^2 n(\mathbf{x},\theta)-\overline{D}\overline{\varepsilon}\mathbf{e}_\theta\cdot\nabla n(\mathbf{x},\theta). \tag{S18}$$

Merging the diffusive terms together, we obtain

$$I_{\text{hop}} = \frac{\overline{D}}{4}\nabla^2 n(\mathbf{x},\theta) + \frac{\overline{D}\overline{\varepsilon}}{4}\nabla\cdot\begin{pmatrix}\cos 2\theta & \sin 2\theta \\ \sin 2\theta & -\cos 2\theta\end{pmatrix}\nabla n(\mathbf{x},\theta) - \overline{D}\overline{\varepsilon}\mathbf{e}_\theta\cdot\nabla n(\mathbf{x},\theta). \tag{S19}$$

Now, we calculate the flipping term I_{flip}. We only keep the first-order terms in the $|\mathbf{m}_i| \ll \rho_i$ expansion. At the leading order, we may suppose

$$W_{\text{flip}}(\theta,\theta') \simeq \gamma \exp\left[\frac{\beta J}{\rho}\mathbf{m}\cdot(\mathbf{e}_\theta - \mathbf{e}_{\theta'})\right] \tag{S20}$$

and the Taylor expansion gives

$$W_{\text{flip}}(\theta,\theta') \simeq \gamma\left[1 + \frac{\beta J}{\rho}\mathbf{m}\cdot(\mathbf{e}_\theta - \mathbf{e}_{\theta'}) + \frac{1}{2}\left(\frac{\beta J}{\rho}\right)^2\left[\mathbf{m}\cdot(\mathbf{e}_\theta - \mathbf{e}_{\theta'})\right]^2 + \frac{1}{6}\left(\frac{\beta J}{\rho}\right)^3\left[\mathbf{m}\cdot(\mathbf{e}_\theta - \mathbf{e}_{\theta'})\right]^3\right]. \tag{S21}$$

Then, the flipping term writes

$$I_{\text{flip}} = \frac{\gamma}{q-1}\sum_{\theta'}\left\{[n(\mathbf{x},\theta') - n(\mathbf{x},\theta)] - \frac{\beta J}{\rho}\left[\mathbf{m}\cdot(\mathbf{e}_{\theta'} - \mathbf{e}_\theta)\right][n(\mathbf{x},\theta') + n(\mathbf{x},\theta)]\right.$$
$$\left. + \frac{1}{2}\left(\frac{\beta J}{\rho}\right)^2\left[\mathbf{m}\cdot(\mathbf{e}_{\theta'} - \mathbf{e}_\theta)\right]^2[n(\mathbf{x},\theta') - n(\mathbf{x},\theta)] - \frac{1}{6}\left(\frac{\beta J}{\rho}\right)^3\left[\mathbf{m}\cdot(\mathbf{e}_{\theta'} - \mathbf{e}_\theta)\right]^3[n(\mathbf{x},\theta') + n(\mathbf{x},\theta)]\right\}. \tag{S22}$$

The first term in Eq. (S22) writes

$$\sum_{\theta'}[n(\mathbf{x},\theta') - n(\mathbf{x},\theta)] = \frac{q}{2\pi}[\rho - 2\pi n], \tag{S23}$$

where we have simplified the notations: $\rho \equiv \rho(\mathbf{x})$ and $n \equiv n(\mathbf{x},\theta)$. The second term in Eq. (S22) writes

$$\sum_{\theta'}\left[\mathbf{m}\cdot(\mathbf{e}_{\theta'} - \mathbf{e}_\theta)\right][n(\mathbf{x},\theta') + n(\mathbf{x},\theta)] = \frac{q}{2\pi}\left[\mathbf{m}^2 - (\rho + 2\pi n)(\mathbf{m}\cdot\mathbf{e}_\theta)\right], \tag{S24}$$

where $\mathbf{m} \equiv \mathbf{m}(\mathbf{x})$. The third term in Eq. (S22) writes

$$\sum_{\theta'}\left[\mathbf{m}\cdot(\mathbf{e}_{\theta'} - \mathbf{e}_\theta)\right]^2[n(\mathbf{x},\theta') - n(\mathbf{x},\theta)] = \frac{q}{2\pi}\left[\frac{1}{2}\mathbf{m}\cdot Q\mathbf{m} - 2\mathbf{m}^2(\mathbf{m}\cdot\mathbf{e}_\theta) + \frac{1}{2}(\rho - 2\pi n)\left(\mathbf{m}^2 + 2(\mathbf{m}\cdot\mathbf{e}_\theta)^2\right)\right], \tag{S25}$$

where $Q \equiv Q(\mathbf{x})$. The fourth term in Eq. (S22) writes

$$\sum_{\theta'}\left[\mathbf{m}\cdot(\mathbf{e}_{\theta'} - \mathbf{e}_\theta)\right]^3[n(\mathbf{x},\theta') + n(\mathbf{x},\theta)] = -\frac{3q}{4\pi}\left[\mathbf{m}\cdot Q\mathbf{m} + (\rho + 2\pi n)\left(\mathbf{m}^2 + \frac{2}{3}(\mathbf{m}\cdot\mathbf{e}_\theta)^2\right)\right](\mathbf{m}\cdot\mathbf{e}_\theta). \tag{S26}$$

Merging all these terms together, the Eq. (S22) becomes

$$I_{\text{flip}} = \frac{q\gamma}{2\pi(q-1)}\left\{[\rho - 2\pi n] - \frac{\beta J}{\rho}\left[\mathbf{m}^2 - (\rho + 2\pi n)(\mathbf{m}\cdot\mathbf{e}_\theta)\right]\right.$$
$$+ \frac{1}{2}\left(\frac{\beta J}{\rho}\right)^2\left[\frac{1}{2}\mathbf{m}\cdot Q\mathbf{m} - 2\mathbf{m}^2(\mathbf{m}\cdot\mathbf{e}_\theta) + \frac{1}{2}(\rho - 2\pi n)\left(\mathbf{m}^2 + 2(\mathbf{m}\cdot\mathbf{e}_\theta)^2\right)\right]$$
$$\left. + \frac{1}{4}\left(\frac{\beta J}{\rho}\right)^3\left[\mathbf{m}\cdot Q\mathbf{m} + (\rho + 2\pi n)\left(\mathbf{m}^2 + \frac{2}{3}(\mathbf{m}\cdot\mathbf{e}_\theta)^2\right)\right](\mathbf{m}\cdot\mathbf{e}_\theta)\right\}, \tag{S27}$$

and the hydrodynamic equation writes

$$\begin{aligned}\frac{\partial n}{\partial t} &= \frac{\overline{D}}{4}\nabla^2 n + \frac{\overline{D}\overline{\varepsilon}}{4}\nabla\cdot\begin{pmatrix}\cos 2\theta & \sin 2\theta\\ \sin 2\theta & -\cos 2\theta\end{pmatrix}\nabla n - \overline{D}\overline{\varepsilon}\mathbf{e}_\theta\cdot\nabla n\\ &+\frac{q\gamma}{2\pi(q-1)}\left\{[\rho-2\pi n]-\frac{\beta J}{\rho}\left[\mathbf{m}^2-(\rho+2\pi n)\,(\mathbf{m}\cdot\mathbf{e}_\theta)\right]\right.\\ &+\frac{1}{2}\left(\frac{\beta J}{\rho}\right)^2\left[\frac{1}{2}\mathbf{m}\cdot Q\mathbf{m}-2\mathbf{m}^2(\mathbf{m}\cdot\mathbf{e}_\theta)+\frac{1}{2}\,(\rho-2\pi n)\left(\mathbf{m}^2+2(\mathbf{m}\cdot\mathbf{e}_\theta)^2\right)\right]\\ &\left.+\frac{1}{4}\left(\frac{\beta J}{\rho}\right)^3\left[\mathbf{m}\cdot Q\mathbf{m}+(\rho+2\pi n)\left(\mathbf{m}^2+\frac{2}{3}(\mathbf{m}\cdot\mathbf{e}_\theta)^2\right)\right](\mathbf{m}\cdot\mathbf{e}_\theta)\right\}.\end{aligned} \tag{S28}$$

This equation for $n(\mathbf{x},\theta)$ depends on the integrated quantities $\rho(\mathbf{x})$, $\mathbf{m}(\mathbf{x})$ and $Q(\mathbf{x})$. To have closed equations, we derive now the equations for these integrated functions.

The density $\rho(\mathbf{x})$ fulfills the equation

$$\partial_t\rho = \frac{\overline{D}}{4}\nabla^2\rho + \frac{\overline{D}\overline{\varepsilon}}{4}\nabla\cdot(\nabla\cdot Q) - \overline{D}\overline{\varepsilon}\nabla\cdot\mathbf{m} \tag{S29}$$

since $\sum_\theta I_{\rm flip}=0$ (statement also verified from Eq. (S27)).

We now derive the equation for the magnetization $\mathbf{m}(\mathbf{x})$. First, we obtain

$$\Delta\theta\sum_\theta \mathbf{e}_\theta I_{\rm hop} = \frac{\overline{D}}{4}\nabla^2\mathbf{m} + \frac{\overline{D}\overline{\varepsilon}}{8}\begin{pmatrix}\partial_{xx}-\partial_{yy} & 2\partial_{xy}\\ 2\partial_{xy} & -\partial_{xx}+\partial_{yy}\end{pmatrix}\mathbf{m} - \frac{\overline{D}\overline{\varepsilon}}{2}\left(\nabla\rho+\nabla\cdot Q\right). \tag{S30}$$

Then, to calculate $\Delta\theta\sum_\theta \mathbf{e}_\theta I_{\rm flip}$, we need the expressions of

$$\Delta\theta\sum_\theta \mathbf{e}_\theta(\mathbf{m}\cdot\mathbf{e}_\theta) = \pi\mathbf{m}, \qquad \Delta\theta\sum_\theta n\mathbf{e}_\theta(\mathbf{m}\cdot\mathbf{e}_\theta) = \frac{1}{2}(\rho+Q)\mathbf{m}, \tag{S31}$$

$$\Delta\theta\sum_\theta \mathbf{e}_\theta(\mathbf{m}\cdot\mathbf{e}_\theta)^2 = 0, \qquad \Delta\theta\sum_\theta n\mathbf{e}_\theta(\mathbf{m}\cdot\mathbf{e}_\theta)^2 = \frac{3}{4}\mathbf{m}^2\mathbf{m}, \tag{S32}$$

$$\Delta\theta\sum_\theta \mathbf{e}_\theta(\mathbf{m}\cdot\mathbf{e}_\theta)^3 = \frac{3\pi}{4}\mathbf{m}^2\mathbf{m}, \qquad \Delta\theta\sum_\theta n\mathbf{e}_\theta(\mathbf{m}\cdot\mathbf{e}_\theta)^3 = \frac{3}{8}\rho\mathbf{m}^2\mathbf{m}. \tag{S33}$$

The first term in Eq. (S27) gives

$$\Delta\theta\sum_\theta \mathbf{e}_\theta\left[\rho-2\pi n\right] = -2\pi\mathbf{m}, \tag{S34}$$

the second term in Eq. (S27) gives

$$\Delta\theta\sum_\theta \mathbf{e}_\theta\left[\mathbf{m}^2-(\rho+2\pi n)\,(\mathbf{m}\cdot\mathbf{e}_\theta)\right] = -2\pi\rho\mathbf{m}-\pi Q\mathbf{m}, \tag{S35}$$

the third term in Eq. (S27) gives

$$\Delta\theta\sum_\theta \mathbf{e}_\theta\left[\frac{1}{2}\mathbf{m}\cdot Q\mathbf{m}-2\mathbf{m}^2(\mathbf{m}\cdot\mathbf{e}_\theta)+\frac{1}{2}\,(\rho-2\pi n)\left(\mathbf{m}^2+2(\mathbf{m}\cdot\mathbf{e}_\theta)^2\right)\right] = -\frac{9\pi}{2}\mathbf{m}^2\mathbf{m}, \tag{S36}$$

and the forth term in Eq. (S27) gives

$$\Delta\theta\sum_\theta \mathbf{e}_\theta\left[\mathbf{m}\cdot Q\mathbf{m}+(\rho+2\pi n)\left(\mathbf{m}^2+\frac{2}{3}(\mathbf{m}\cdot\mathbf{e}_\theta)^2\right)\right](\mathbf{m}\cdot\mathbf{e}_\theta) = 3\pi\rho\mathbf{m}^2\mathbf{m}. \tag{S37}$$

We obtain then

$$\Delta\theta \sum_{\theta} \mathbf{e}_\theta I_{\text{flip}} = \frac{q\gamma}{q-1}\left[(\beta J - 1) - \frac{3}{2}\left(\frac{\beta J}{2\rho}\right)^2 (3-\beta J)\mathbf{m}^2 + \frac{\beta J}{2\rho} Q\right]\mathbf{m}, \tag{S38}$$

and the magnetization $\mathbf{m}(\mathbf{x})$ fulfills the equation

$$\begin{aligned}\partial_t \mathbf{m} = \frac{\overline{D}}{4}\nabla^2\mathbf{m} + \frac{\overline{D}\overline{\varepsilon}}{8}\begin{pmatrix}\partial_{xx}-\partial_{yy} & 2\partial_{xy}\\ 2\partial_{xy} & -\partial_{xx}+\partial_{yy}\end{pmatrix}\mathbf{m} - \frac{\overline{D}\overline{\varepsilon}}{2}(\nabla\rho + \nabla\cdot Q)\\ + \frac{q\gamma}{q-1}\left[(\beta J - 1) - \frac{3}{2}\left(\frac{\beta J}{2\rho}\right)^2 (3-\beta J)\mathbf{m}^2 + \frac{\beta J}{2\rho} Q\right]\mathbf{m}.\end{aligned} \tag{S39}$$

The expression of the nematic tensor $Q(\mathbf{x})$ is obtained by neglecting the diffusion and drift terms. From Eq. (II), the nematic tensor fulfills then

$$\dot{Q} = \frac{q\gamma}{2\pi(q-1)}\left[-2\pi Q + \frac{\beta J}{\rho}\Delta\theta \sum_{\theta}\begin{pmatrix}\cos 2\theta & \sin 2\theta\\ \sin 2\theta & -\cos 2\theta\end{pmatrix}(\rho + 2\pi n)(\mathbf{m}\cdot\mathbf{e}_\theta)\right]. \tag{S40}$$

Assuming $\dot{Q} = 0$, we obtain

$$Q = \frac{\beta J}{2\rho}\begin{pmatrix}m_x^2 - m_y^2 & 2m_x m_y\\ 2m_x m_y & -m_x^2 + m_y^2\end{pmatrix}. \tag{S41}$$

We can deduce then

$$Q\mathbf{m} = \frac{\beta J}{2\rho}\mathbf{m}^2\mathbf{m}, \tag{S42}$$

and the equation for the magnetization becomes

$$\begin{aligned}\partial_t \mathbf{m} = \frac{\overline{D}}{4}\nabla^2\mathbf{m} + \frac{\overline{D}\overline{\varepsilon}}{8}\begin{pmatrix}\partial_{xx}-\partial_{yy} & 2\partial_{xy}\\ 2\partial_{xy} & -\partial_{xx}+\partial_{yy}\end{pmatrix}\mathbf{m} - \frac{\overline{D}\overline{\varepsilon}}{2}(\nabla\rho + \nabla\cdot Q)\\ + \frac{q\gamma}{q-1}\left[(\beta J - 1) - \frac{1}{2}\left(\frac{\beta J}{2\rho}\right)^2 (7-3\beta J)\mathbf{m}^2\right]\mathbf{m}.\end{aligned} \tag{S43}$$

The equations obtained for the density and the magnetization are not yet averaged over stochastic realizations. We consider that the magnetization follows a Gaussian distribution such that

$$P(\mathbf{m}) = \frac{1}{2\pi\sigma^2}\exp\left[-\frac{(\mathbf{m}-\boldsymbol{\mu})^2}{2\sigma^2}\right], \tag{S44}$$

where $\langle\mathbf{m}\rangle = \boldsymbol{\mu}$, $\langle\mathbf{m}^2\rangle = \boldsymbol{\mu}^2 + 2\sigma^2$. We obtain then $\langle\mathbf{m}^2\mathbf{m}\rangle = \boldsymbol{\mu}^2\boldsymbol{\mu} + 4\sigma^2\boldsymbol{\mu}$, and

$$Q = \frac{\beta J}{2\rho}\begin{pmatrix}\mu_x^2 - \mu_y^2 & 2\mu_x\mu_y\\ 2\mu_x\mu_y & -\mu_x^2 + \mu_y^2\end{pmatrix}. \tag{S45}$$

We have shown in the main text that $\sigma \propto \rho^{\xi}$ (with $1 \leqslant \xi \leqslant 1.67$), which gives the hydrodynamic equations:

$$\partial_t \langle \rho \rangle = \frac{\overline{D}}{4} \nabla^2 \langle \rho \rangle + \frac{\overline{D}\bar{\varepsilon}}{4} \nabla \cdot (\nabla \cdot Q) - \overline{D}\bar{\varepsilon} \nabla \cdot \langle \mathbf{m} \rangle, \tag{S46}$$

$$\partial_t \langle \mathbf{m} \rangle = \frac{\overline{D}}{4} \nabla^2 \langle \mathbf{m} \rangle + \frac{\overline{D}\bar{\varepsilon}}{8} \begin{pmatrix} \partial_{xx} - \partial_{yy} & 2\partial_{xy} \\ 2\partial_{xy} & -\partial_{xx} + \partial_{yy} \end{pmatrix} \langle \mathbf{m} \rangle - \frac{\overline{D}\bar{\varepsilon}}{2} \left(\nabla \langle \rho \rangle + \nabla \cdot Q \right)$$
$$+ \frac{q\gamma}{q-1} \left[(\beta J - 1 - r \langle \rho \rangle^{\alpha}) - \frac{1}{2} \left(\frac{\beta J}{2 \langle \rho \rangle} \right)^2 (7 - 3\beta J) \langle \mathbf{m} \rangle^2 \right] \langle \mathbf{m} \rangle, \tag{S47}$$

$$Q = \frac{\beta J}{2 \langle \rho \rangle} \begin{pmatrix} \langle m_x \rangle^2 - \langle m_y \rangle^2 & 2 \langle m_x \rangle \langle m_y \rangle \\ 2 \langle m_x \rangle \langle m_y \rangle & -\langle m_x \rangle^2 + \langle m_y \rangle^2 \end{pmatrix}, \tag{S48}$$

with $\alpha = \xi - 2$ and where r is a constant which usually depends on β. These equations are reported in main text as Eqs. (3)-(5) where the stochastic average $\langle \cdots \rangle$ have been omitted. When $r = 0$, the mean-field equations are recovered, and we can take $r = 1$ without any loss of generality (up to a rescaling of the density and the magnetization). We may note that

$$\nabla \cdot Q = -\frac{\nabla \langle \rho \rangle}{\langle \rho \rangle} \cdot Q + \frac{\beta J}{\langle \rho \rangle} \left[(\langle \mathbf{m} \rangle \cdot \nabla) \langle \mathbf{m} \rangle - (\langle \mathbf{m}_{\perp} \rangle \cdot \nabla) \langle \mathbf{m}_{\perp} \rangle \right] \tag{S49}$$

with $\mathbf{m} = (m_x, m_y)$ and $\mathbf{m}_{\perp} = (-m_y, m_x)$.

III. ALGORITHM TO OBTAIN THE TIME-AVERAGED PROFILES

Here, we would like to briefly discuss the algorithm that has been used to obtain the time-averaged density profiles in Fig. 2(c). For each instantaneous density profile k at time t, we first move the center of each of the n_b stripes ($n_b > 1$) to a fixed point x_0 on the x-axis by doing a coordinate shifting (we always consider $x_0 = L_x/2$) and perform an averaging over these stripes at time t. We then denote the averaged density over these stripes by $\bar{\rho}_k(x)$. We repeat this procedure for $n_p \simeq 200 - 300$ such instantaneous profiles and finally perform a thermal averaging over n_p number of $\bar{\rho}_k(x)$ to obtain the time-averaged density profile as $\langle \bar{\rho}(x) \rangle = \frac{1}{n_p} \sum_{k=1}^{n_p} \bar{\rho}_k(x)$.

IV. ORDER PARAMETER DISTRIBUTION AS A FUNCTION OF ρ_0 FOR $q = 7$

Distribution of the order parameter for a fixed q and several densities are shown in Fig. S6 for $q = 7$, $\beta = 2$ and $\bar{\varepsilon} = 0$ where we observe all the three different phases as a function of ρ_0: (a–b) homogeneous disordered phase with uniform distribution of spins at small ρ_0, where every spin points to a random direction, (c)–(e) a QLRO phase at intermediate densities with a ringlike distribution of the order parameter and (f) a LRO phase at a sufficiently high density where seven distinct spots correspond to the seven possible ordering states. One can notice that the spread of the distribution around the angles allowed for the clock spins in the LRO phase of $q = 7$ is greater compared to $q = 4$ and $q = 5$ in Fig. 4 and things like the system size or the higher degeneracy of the state (due to which a perfect LRO phase like Fig. 4(a)–(b) might only be possible at a larger density) might be responsible for this. The conclusion which we draw from Fig. S6 is that the liquid phase for discrete q values and for $\bar{\varepsilon} = 0$ shows both QLRO and LRO at different parameter regimes, QLRO at smaller ρ_0 [$\rho_0 > \rho^*(q)$] and LRO at a larger ρ_0. As shown in the context of equilibrium q-state clock models [3], one can also expect such a scenario as a function of temperature β.

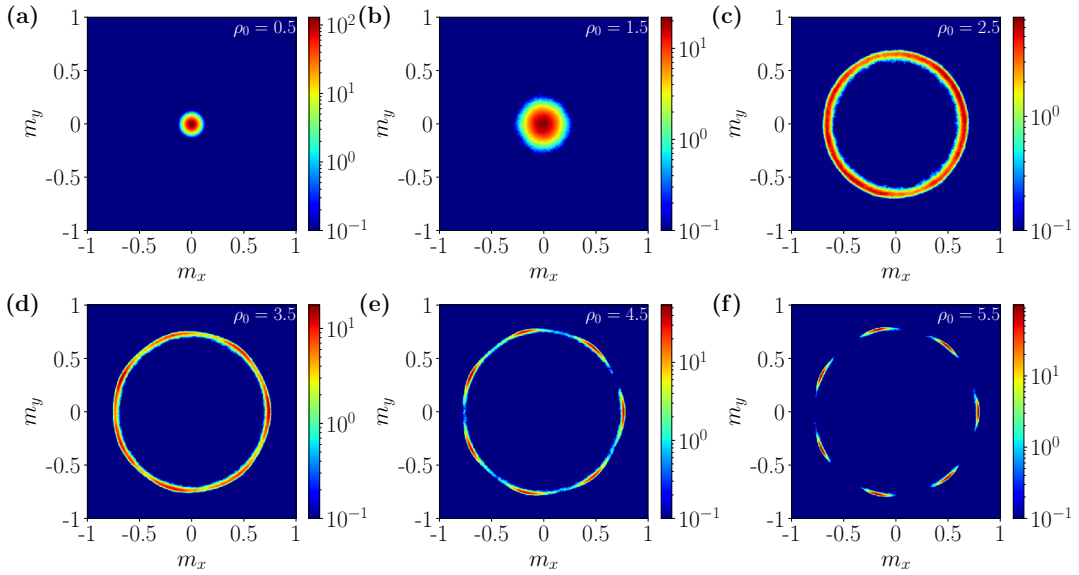

FIG. S6: (color online) Order parameter distributions for $q = 7$ and several ρ_0 values. Parameters: $L = 50$, $\beta = 2$ and $\bar{\varepsilon} = 0$.

V. EFFECTIVE EXPONENTS AS A FUNCTION OF q

In Fig. S7(a) and Fig. S7(b), we respectively present the effective exponents $\xi_n^{\rm eff} = d[\ln(\Delta n^2)]/d[\ln\langle n\rangle]$ and $\xi_m^{\rm eff} = d[\ln(\Delta m^2)]/d[\ln\langle n\rangle]$ versus average particle number $\langle n\rangle$ (where n denotes the particle number in subsystems of linear size ℓ) for several q values corresponding to the number fluctuations and magnetization fluctuations shown in Fig. 4(a)-(b). The exponents in Table 1 have been obtained by fitting the data in Fig. 4(a)–(b) to a power-law and since the extracted exponents depend on the interval along the x-axis to which the fits are restricted, a look at the log-log slope of the data or the effective exponent reveals more insight. The plots show "plateaus" around the extracted exponents for the corresponding q values (see Table 1) for at most one decade of $\langle n\rangle$ and then $\xi^{\rm eff}$ decreases with increasing $\langle n\rangle$ when $\langle n\rangle$ approaches the total number of particles in the system and becomes smaller than 1 due to the finite-size cut-off at $\langle n\rangle = N = \rho_0 L^2$, where Δn^2 vanishes.

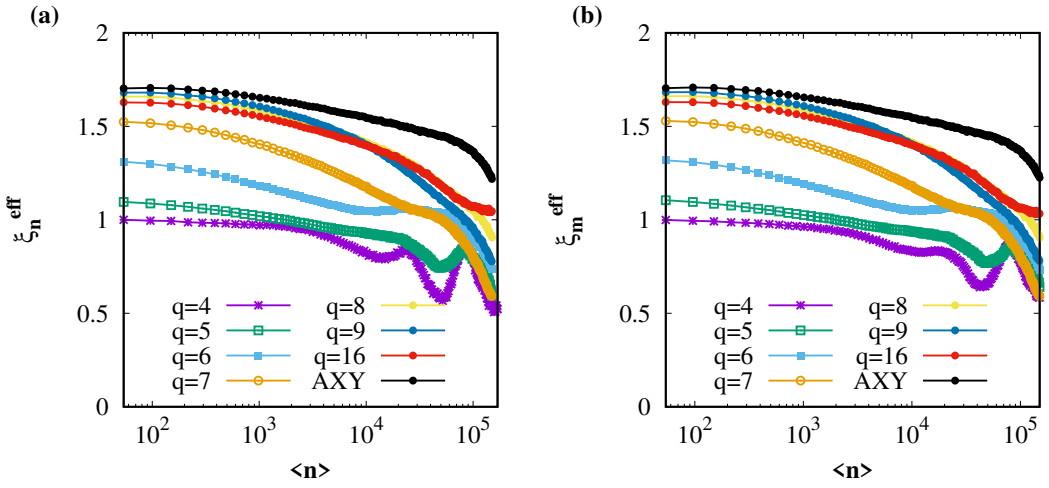

FIG. S7: (color online) (a)–(b) Effective exponents $\xi_n^{\rm eff}$ and $\xi_m^{\rm eff}$ versus $\langle n\rangle$ for the data plotted in Fig. 4(a)-(b). Parameters: $\beta = 2$, $\bar{\varepsilon} = 0.9$, and $\rho_0 = 6$.

[1] S. Chatterjee, M. Mangeat, R. Paul, and H. Rieger, *Flocking and re-orientation transition in the q-state active Potts model*, EPL **130**, 6 (2020); M. Mangeat, S. Chatterjee, R. Paul, and H. Rieger, *Flocking with a q-fold discrete symmetry: band-to-lane transition in the active Potts model*, Phys. Rev. E **102**, 042601 (2020).

[2] A. P. Solon and J. Tailleur, *Revisiting the flocking transition using active spins*, Phys. Rev. Lett. **111**, 078101 (2013); *Flocking with discrete symmetry: The two-dimensional active Ising model*, Phys. Rev. E **92**, 042119 (2015).

[3] S. Chatterjee, S. Puri, and R. Paul, *Ordering kinetics in the q-state clock model: Scaling properties and growth laws*, Phys. Rev. E **98**, 032109 (2018).